VOL. 6, NO. 1 (March 2026) 1-24
https://jagst.utm.my

JAGST
Journal of Advanced Geospatial Science & Technology

Plate Tectonic Calculator: Stand-Alone Application for Estimating Plate Tectonic Motion over the Earth's Surface

Ahmad Zikri Abd Aziz[1*], Mohamad Asrul Mustafar[1], Mohd Azwan Abbas[1], Norshahrizan Mohd Hashim[1], Soeb Nordin[2]

[1]Faculty of Built Environment, Universiti Teknologi MARA, Perlis Branch, Arau Campus, 02600 Arau, Perlis, Malaysia
[2]Geodetic Solution Sdn Bhd, No.33-1, Jalan Komersial Senawang 7, 70450 Seremban, Negeri Sembilan, Malaysia

*Corresponding author: ahmadzikriabdaziz@gmail.com

Abstract **–** Plate tectonic motion is the displacement of the plates over the earth's surface. Significant displacements can be detected in regions with high seismic activity. Following Euler's theorem, continental plates rotate about an axis that runs through the center of the earth's sphere. Therefore, plate tectonic motion is emphasised, with the rate of movement calculated annually. Hence, this study aims to develop a stand-alone application to calculate plate tectonic motion concerning Euler's theorem. A plate tectonic calculator (PTC) is designed using optimised parameters and formulations that can calculate motion in any region. Furthermore, the set of formulations from Euler's theorem that have been revised into a comprehensive form is verified using manual calculation in MATLAB. The formulations are categorized into two stages: the inverse Euler pole problem in the Local Geodetic Coordinate System (LG CS) and the direct Euler pole problem in LG CS. After integrating the PTC in C# using Visual Studio, the sample coordinates and velocities of stations from four case datasets are used to test the PTC's performance. Moreover, the effectiveness of the PTC is further assessed by comparing its outputs with those of the existing Euler Pole Calculator (EPC). The results show no significant differences in any parameter across all cases. This is because the differences are too small and within uncertainties, and also do not exceed the tolerance range of the standard deviation for each parameter involved. The graph of the velocity differences between PTC and EPC indicates the discrepancies are less than 1×10^{-6} meters per year, whereas the velocity residuals and standard deviation show the same discrepancies that are less than 1×10^{-9} meters per year. Consequently, it can be concluded that the PTC's performance has been successfully verified. In addition, it can more effectively detect plate tectonic motion within the given region.

Keywords *– Plate Tectonic, Euler's Theorem, Calculator, Euler Pole*

Article History: Received 4 January 2026, Accepted 2 March 2026, Published 31 March 2026

How to cite: Abd Aziz, A. Z., Mustafar, M. A., Abbas, M. A., Hashim, N. M. and Nordin, S. (2026). Plate Tectonic Calculator: Stand-Alone Application for Estimating Plate Tectonic Motion over the Earth's Surface. Journal of Advanced Geospatial Science and Technology. 6(1), 1-24. https://doi.org/10.11113/jagst.v6n1.126

1.0 Introduction

The Global Navigation Satellite System (GNSS) has been introduced specifically for geodynamics, which focuses on the study of the earth's surface. According to Li et al. (2022), advanced satellite positioning technology has been utilised to operate GNSS systems to obtain satellite data. Here, continuous stations have been established worldwide to study the geodynamics underlying sustained tectonic motion. It is undeniable that the deformation on the earth's surface always occurs either in a small way or more significantly, depending on the seismicity of a region. For example, we can observe the tectonic plate in North Borneo, where this region continues to show a gradual clockwise rotation relative to the Sundaland blocks (Mustafar et al., 2017). This study focuses on the concept of plate tectonics in a region, considering the most efficient processes involved. McCubbine et al. (2024) explained that the motion of tectonic plates is presently parameterised on a spherical geometry through Euler's theorem, which applies the concept of Euler pole parameters (EPPs). By referring to Euler's theorem, the axis of the rotation's pole and the surface of the sphere are the two points that intersect with each other (Lowrie & Fichtner, 2020). This theorem allows for locating any region to resolve the tectonic plate in space. Therefore, the analysis of intraplate motions can be performed. Previously, plate motion models successfully compared estimates from different sources, including hotspot tracks, space geodetic measurements, ocean-ridge spreading rates, earthquake slip vectors, and transform-fault azimuths (Goudarzi et al., 2014).

Despite the critical necessity of Euler pole computations in geodynamic research, only a few applications have been established to calculate the EPPs from absolute velocity data. For instance, Goudarzi et al. (2014) developed the Euler Pole Calculator (EPC) in MATLAB, whereas Tamaki & Okino (2018) and Andrews (2003) developed the Plate Motion Calculator and the Rice University Plate Motion Calculator, respectively, via online websites. In addition, the GAGE Plate Motion Calculator by UNAVCO and the Plate Motion Calculator by Barcelona Field Studies Centre are also executable as online software. Nevertheless, some complications arise when accessing existing applications, since most lack user-friendliness. Two accessibility issues have been identified: applications need to be accessed via an online website, and some require an intermediary software platform to run. Therefore, this study develops a stand-alone application that is more efficient and can be executed in offline mode by applying the mathematical background of Euler's theorem. This approach will be more effective at encouraging users to

benefit from this application, as they can access it directly without additional software or an internet connection.

Apart from that, the subsequent issue concerns the platform to be used for designing and integrating the application for the development phase. As we know, MATLAB is highly recommended, especially for computational studies. However, there are some restrictions on MATLAB, the major issue being the license (Evora et al., 2024). In this case, users need a license to use MATLAB itself and to integrate the application. Besides, the minor issue with MATLAB is its installation memory requirements, which require a large amount of memory (Adewale et al., 2021). Hereby, all these issues have been highlighted to justify the use of publicly available, open-source Visual Studio software. Hereby, new software development remains relevant, as it can enhance the model's solution performance and enable model evaluation by comparing outputs from various software (Goudarzi et al., 2014). In addition, not all the software is freely distributable across all operating systems. Therefore, this research aims to develop a new application called the Plate Tectonic Calculator (PTC). Aside from Global Positioning System (GPS) velocity vectors, the application can also be utilised with other methods of obtaining velocity vectors.

2.0 The Concept of Plate Tectonic Motion

Plate tectonics is a core principle of geological science that explains the extensive movement of the earth's outer shell, the lithosphere. The theory elucidates a range of geological processes, including seismic activity, volcanism, mountain formation, and the development of oceanic trenches. These lithospheric plates interact primarily at their edges, where three types of movements, including divergent, convergent, and transform, define their behavior. Each boundary type leads to unique geological outcomes, reflecting the dynamic character of earth's crustal evolution (Chen et al., 2020). Divergent boundaries mark regions where tectonic plates drift apart, allowing magma from the mantle to rise and solidify as new oceanic crust. This mechanism is most prominently observed along mid-ocean ridges, where ongoing seafloor spreading drives the expansion of ocean basins (Aneeshkumar et al., 2022).

In contrast, convergent plate interactions involve the collision of lithospheric plates, resulting in either subduction, where one plate is forced beneath another, or continental collision.

Transform plate boundaries are characterised by lateral movement, where adjacent plates grind past one another. These interactions typically build up tectonic stress, which is eventually released as earthquakes along fault zones (Blas et al., 2022).

The earth's surface is in a continuous state of change, driven primarily by the dynamic behavior of tectonic plates within the lithosphere. According to the National Oceanic and Atmospheric Administration (NOAA, 2024), the lithosphere comprises approximately 15 to 20 major plates that rest atop the earth's semi-molten mantle. These plates resemble interlocking segments of a fragmented shell and are driven by internal heat generated by radioactive decay. This energy source causes the plates to shift over time, sometimes in opposing directions. Over millennia, as the earth's mantle heated and cooled, the outer crust fractured, initiating the plate motion that continues today. The massive continent eventually disintegrated, forming new land masses and oceans. The earth's land masses migrate in opposite directions at an average rate of around 15.2 millimeters per year (NOAA, 2024). Every tectonic plate can be considered a rigid body on the surface of a sphere. Following Euler's theorem, continental plates rotate about an axis that passes through the center of the earth's sphere, as shown in Figure 1. The rotation axes cross at these sites, forming the Euler pole. There is only one angular velocity vector that begins at the center of the globe that may be used to describe plate motion. A vector containing the latitude and longitude of where the rotation axis crosses the earth's surface can be used to parameterize the rotation rate equal to the magnitude of the angular velocity of the earth's rotation axis (in degrees per million years or microradians per year). When calculating EPPs, the angular velocity vector and rotation pole (latitude and longitude) are taken into consideration. Figural representation of the angular motion of a single plate depicted as a succession of little circles. When viewed through the lens of the rotating pole coordinate system, the earth's conventional geographic coordinate system, which includes parallels and meridians, appears to be inclined (Müller & Seton, 2016).

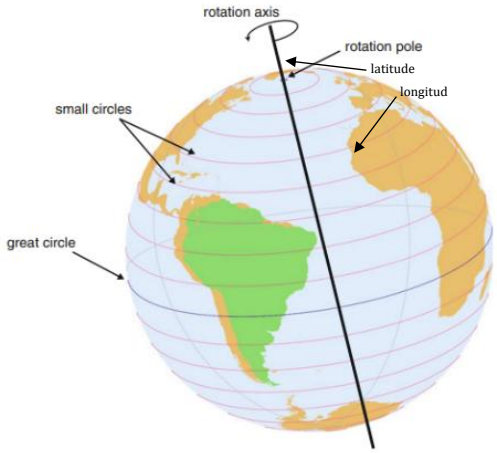

Figure 1. Concept of Euler's Theorem (Müller & Seton, 2016)

One of the primary drivers of tectonic movement is mantle convection, a process in which heat from the earth's interior circulates within the mantle. This internal movement imparts force to the overlying plates, contributing to their motion through mechanisms such as slab pull and ridge push. Slab pull arises from the gravitational descent of cooler, denser lithospheric plates into the mantle, while ridge push is driven by the elevation of lithosphere near mid-ocean ridges (Zhou & Wada, 2022). Tectonic plate motions significantly influence biodiversity and climate. Plate movements can create or destroy habitats, affecting species distribution and ecological connectivity.

Additionally, changes in continental configurations and topography alter oceanic and atmospheric circulation, thereby contributing to long-term climate variability (Zhang et al., 2024). The geological record, including sediment layers, fossil locations, and rock formations, serves as a vital archive of past tectonic events. These records allow scientists to reconstruct historical plate movements and understand the shifting arrangement of ancient landmasses (Jagoda, 2021). Tectonic plate dynamics are influenced by a complex set of factors, ranging from deep mantle processes to interactions at surface boundaries. These movements constantly reshape earth's structure and contribute to broader environmental and ecological transformations. The study of plate tectonics remains central to understanding both earth's physical history and its ongoing geodynamic evolution, underscoring its interdisciplinary significance across the sciences (Parsons et al., 2021).

2.1 The Needs of Application Development for Estimating the Plate Tectonic Motion

The creation of an application designed to model and compute tectonic plate motion across earth's surface holds significant importance not only for geodynamic research. Plate tectonics plays a critical role in earthquake genesis, as seismic activity predominantly results from interactions at plate margins. A robust application would incorporate real-time data from geodetic monitoring systems and integrate computational models to evaluate plate kinematics and support seismic forecasting. As stress accumulates at plate interfaces, continuous monitoring could provide early warnings of seismic hazards, thereby mitigating risks to human life and infrastructure (Aneeshkumar et al., 2022). Moreover, such a tool could elucidate the influence of tectonic motion on broader geological processes, including volcanism, mountain formation, and sedimentary dynamics (Collot et al., 2023). For instance, subduction zones, which are associated with intense seismic and volcanic activity, can be analyzed through high-resolution simulations, potentially enhancing the accuracy of eruption predictions and hazard preparedness (Cerpa et al., 2022). The application could support interdisciplinary research, given the pivotal role tectonics plays in shaping environments and influencing climate systems (Zhou & Wada, 2022).

In seismic-prone urban areas, applying tectonic data to infrastructure planning can inform the strategic placement and design of resilient buildings and transport systems (Huang et al., 2021). Predictive modeling of tectonic movement helps minimize damage from seismic events by informing engineering standards and hazard zoning (Koppers et al., 2021). Furthermore, in geologically active regions, the application could inform governmental policy and land-use decisions by providing insight into ongoing tectonic deformation. With a user-friendly design and embedded educational features, the platform could serve as a powerful tool for public engagement, enhancing general awareness of tectonic processes and natural hazard preparedness. Within academic settings, it may function as an interactive teaching aid, transforming abstract geoscience theories into tangible learning experiences (Zhang et al., 2024). The application would also promote collaborative research through centralised data sharing, enabling comparative studies across regions and enhancing global tectonic models. By integrating machine learning, the system could detect trends and generate predictive models of future tectonic scenarios, thereby advancing the frontiers of geoscientific knowledge (Wiel et al., 2024). Ultimately, this platform would address critical societal and scientific demands ranging from hazard mitigation to scientific

discovery, demonstrating the wide-reaching benefits of investing in advanced tectonic modeling technologies (Parsons et al., 2021).

3.0 Calculation Procedures for Application Development

Figure 2 illustrates the calculation procedures for developing the PTC application, which consists of two parts: the inverse Euler pole problem and the direct Euler pole problem, used to compute the EPPs and relative velocities, respectively.

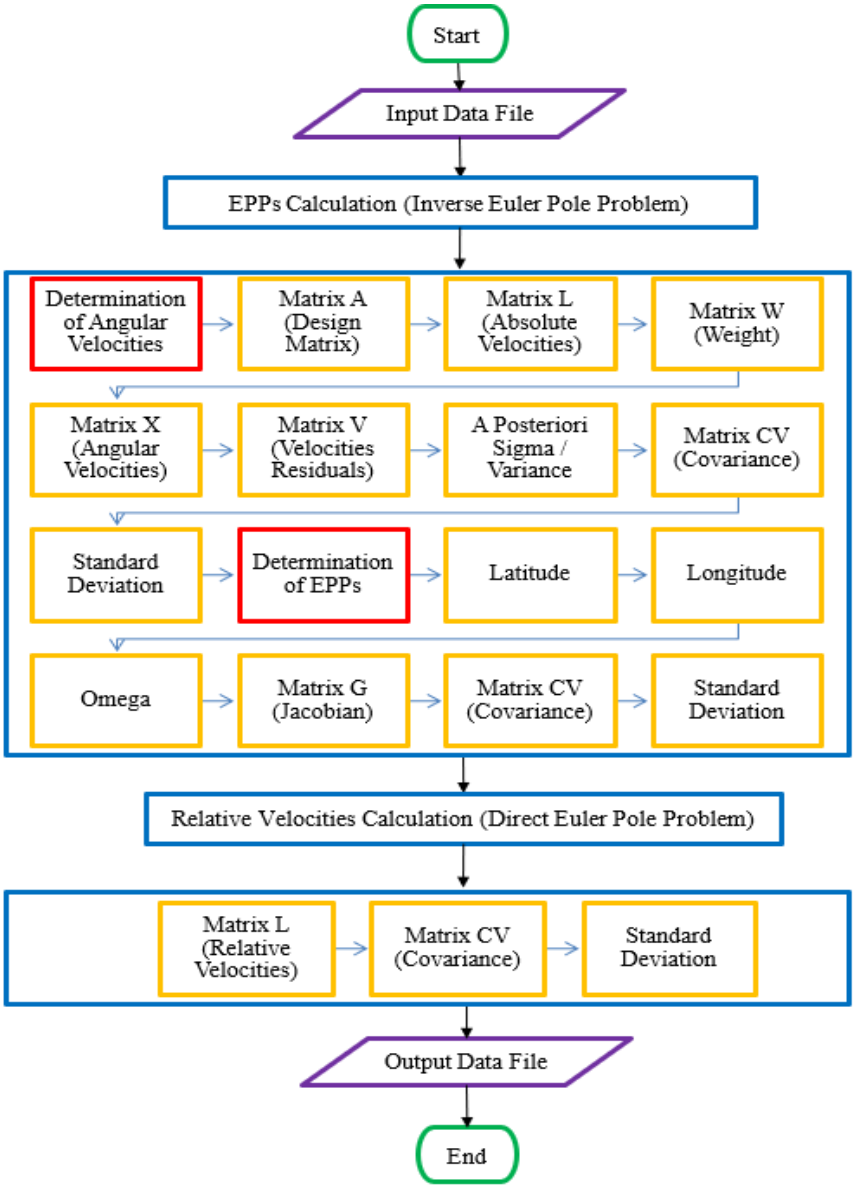

Figure 2. Calculation Procedures for the PTC Development

3.1 Inverse Euler Pole Problem in Local Geodetic Coordinate System (LG CS)

Based on Euler's theorem, the observation equation or velocity vectors for n measuring stations on the same rigid plate p is written as below (Goudarzi et al., 2014).

$$\begin{bmatrix}\mathbf{v}_1\\ \vdots\\ \mathbf{v}_n\end{bmatrix}^P_{2n\times 1} = \begin{bmatrix}\mathbf{X}_1\\ \vdots\\ \mathbf{X}_n\end{bmatrix}^P_{2n\times 3}\begin{bmatrix}\omega_x\\ \omega_y\\ \omega_z\end{bmatrix}^P_{3\times 1} \tag{1}$$

$$\begin{aligned}\mathbf{v}_i^p &= \begin{bmatrix}v_n\\ v_e\end{bmatrix}_{i(LG)}\\ &= r_e\begin{bmatrix}\sin\lambda & -\cos\lambda & 0\\ -\sin\phi\cos\lambda & -\sin\phi\sin\lambda & \cos\phi\end{bmatrix}_i\begin{bmatrix}\omega_x^p\\ \omega_y^p\\ \omega_z^p\end{bmatrix}\\ &= \mathbf{K}_i^{(LG)}\begin{bmatrix}\omega_x^p\\ \omega_y^p\\ \omega_z^p\end{bmatrix}\end{aligned} \tag{2}$$

Hereby, the rotation vector $\boldsymbol{\Omega}^p = \left(\omega_x^p, \omega_y^p, \omega_z^p\right)^T$ for the rigid plate p is computed by applying the least-squares method. If the observation vector $(\mathbf{v}_1 \cdots \mathbf{v}_n)^T$ is shown by $\mathbf{L}$ and the design matrix $(\mathbf{X}_1 \cdots \mathbf{X}_n)^T$ by $\mathbf{A}$, then the formulation is depicted as below:

$$\begin{aligned}\boldsymbol{\Omega}^p &= (\mathbf{A}^T\mathbf{W}\mathbf{A})^{-1}(\mathbf{A}^T\mathbf{W}\mathbf{L})\\ &= \mathbf{N}^{-1}\mathbf{A}^T\mathbf{W}\mathbf{L}\end{aligned} \tag{3}$$

where $\mathbf{W}$ represents the weight matrix of the observations, while $\mathbf{N}^{-1}$ represents the cofactor matrix of unknowns.

The rotation vector expresses the rotation's rate $|\boldsymbol{\Omega}^p|$ (angular velocity) and the rotation's pole (spherical latitude and spherical longitude) by presuming the rotation on a sphere as below:

$$\begin{aligned}|\Omega^p| &= \sqrt{\left(\omega_x^p\right)^2 + \left(\omega_y^p\right)^2 + \left(\omega_z^p\right)^2}\\ \Omega^p_{\text{lat}} &= \arctan\left(\omega_z^p / \sqrt{\left(\omega_x^p\right)^2 + \left(\omega_y^p\right)^2}\right)\\ \Omega^p_{\text{long}} &= \arctan\left(\omega_y^p/\omega_x^p\right)\end{aligned} \tag{4}$$

The standard deviation, or the accuracy of the components, for the estimated rotation vector $\boldsymbol{\Omega}^p\left(\omega_x^p, \omega_y^p, \omega_z^p\right)$ represents the square root of the diagonal elements for the covariance matrix of unknowns $\boldsymbol{\Sigma}_{\boldsymbol{\Omega}^p}$, which is computed by applying the a posteriori sigma value $\hat{\sigma}_0$ as well as the cofactor matrix of unknowns, as below:

$$\boldsymbol{\Sigma}_{\boldsymbol{\Omega}^p} = \hat{\sigma}_0^2 \cdot \mathbf{N}^{-1} \tag{5}$$

then $\hat{\sigma}_0$ is computed as:

$$\hat{\sigma}_0 = \sqrt{\frac{\boldsymbol{v}_r^T \mathbf{W} v_r}{df}} \tag{6}$$

where $\boldsymbol{v}_r$ represents the vector of velocity residuals, while df represents the degree of freedom for the equation system.

Even though there are three observation equations for each velocity vector, the degree of freedom in equation 6 is denoted $2n - 3$, where n is the number of measuring stations. This is due to the third component of the velocity vector being reliant on the first two and thus cannot be regarded as an autonomous observation equation. The radial component of the velocity equivalent to the vertical velocity on the sphere is not added to the solution of the rotation vector. This is demonstrated by equation 2 in the context of LG CS.

The accuracy of the estimated EPPs $\left(|\boldsymbol{\Omega}^p|, \Omega_{\text{lat}}^p, \Omega_{\text{long}}^p\right)$ is defined using the law of error propagation to as below:

$$\boldsymbol{\Sigma}_{\boldsymbol{\omega}^p} = \mathbf{G}\boldsymbol{\Sigma}_{\Omega^p}\mathbf{G}^T \tag{7}$$

where $\mathbf{G}$ represents the Jacobian matrix of the linearised observation:

$$\mathbf{G} = \begin{bmatrix} \frac{\partial|\mathbf{\Omega}^p|}{\partial\omega_x^p} & \frac{\partial|\mathbf{\Omega}^p|}{\partial\omega_y^p} & \frac{\partial|\mathbf{\Omega}^p|}{\partial\omega_z^p} \\ \frac{\partial\phi}{\partial\omega_x^p} & \frac{\partial\phi}{\partial\omega_y^p} & \frac{\partial\phi}{\partial\omega_z^p} \\ \frac{\partial\lambda}{\partial\omega_x^p} & \frac{\partial\lambda}{\partial\omega_y^p} & \frac{\partial\lambda}{\partial\omega_z^p} \end{bmatrix}$$

$$= \begin{bmatrix} \frac{\omega_x^p}{|\mathbf{\Omega}^p|} & \frac{\omega_y^p}{|\mathbf{\Omega}^p|} & \frac{\omega_z^p}{|\mathbf{\Omega}^p|} \\ -\frac{1}{|\mathbf{\Omega}^p|^2} \cdot \frac{\omega_x^p \omega_z^p}{\sqrt{\left(\omega_x^p\right)^2 + \left(\omega_y^p\right)^2}} & -\frac{1}{|\mathbf{\Omega}^p|^2} \cdot \frac{\omega_y^p \omega_z^p}{\sqrt{\left(\omega_x^p\right)^2 + \left(\omega_y^p\right)^2}} & -\frac{1}{|\mathbf{\Omega}^p|^2} \cdot \sqrt{\left(\omega_x^p\right)^2 + \left(\omega_y^p\right)^2} \\ \frac{-\omega_y^p}{\left(\omega_x^p\right)^2 + \left(\omega_y^p\right)^2} & \frac{\omega_x^p}{\left(\omega_x^p\right)^2 + \left(\omega_y^p\right)^2} & 0 \end{bmatrix}$$

Therefore, the sigma values or the accuracy of the estimated velocities are computed by applying the covariance matrix of the rotation vector $\mathbf{\Sigma}_{\boldsymbol{\omega}^p}$ from equation 7.

3.2 Direct Euler Pole Problem in Local Geodetic Coordinate System (LG CS)

Whenever the coordinates of the measuring stations are available in LG CS, the LG CS model is utilised, which relies on the Earth-Centered Earth-Fixed Coordinate System (ECEF CS). $\mathbf{X}_i$ is restructured by employing the conversion between ECEF CS and station spherical coordinates as below:

$$\mathbf{X}_i = r_e \begin{bmatrix} 0 & \sin\,\phi & -\cos\phi\sin\,\lambda \\ -\sin\,\phi & 0 & \cos\phi\cos\,\lambda \\ \cos\phi\sin\,\lambda & -\cos\phi\cos\,\lambda & 0 \end{bmatrix}_i \tag{8}$$

where r_e represents the radius of the earth, which is 6371 kilometers, whereas ϕ and λ represent the spherical latitude and spherical longitude of the station i, respectively.

From the ECEF CS velocity $\mathbf{v}_i^{(\mathrm{ECEF})}$, the LG CS velocity $\mathbf{v}_i^{(\mathrm{LG})}$ is computed via the rotation matrix $\mathbf{R}_i$. The velocity vector in LG CS is provided as equation 9:

$$\mathbf{v}_i^p = \begin{bmatrix} v_n \\ v_e \\ v_u \end{bmatrix}_{i(\mathrm{LG})} = r_e \begin{bmatrix} \sin\lambda & -\cos\lambda & 0 \\ -\sin\phi\cos\lambda & -\sin\phi\sin\lambda & \cos\phi \\ 0 & 0 & 0 \end{bmatrix}_i \begin{bmatrix} \omega_x^p \\ \omega_y^p \\ \omega_z^p \end{bmatrix} \tag{9}$$

Equation 9 clearly illustrates that the velocity vector's up component is zero. This demonstrates that rotation about the Euler pole on a spherical surface does not affect elevation. Thus, equation 9 is simplified, and the horizontal velocities in LG CS are determined as follows:

$$\mathbf{v}_i^p = \begin{bmatrix} v_n \\ v_e \end{bmatrix}_{i(LG)} = r_e \begin{bmatrix} \sin\lambda & -\cos\lambda & 0 \\ -\sin\phi\cos\lambda & -\sin\phi\sin\lambda & \cos\phi \end{bmatrix}_i \begin{bmatrix} \omega_x^p \\ \omega_y^p \\ \omega_z^p \end{bmatrix} = \mathbf{K}_i^{(LG)} \begin{bmatrix} \omega_x^p \\ \omega_y^p \\ \omega_z^p \end{bmatrix} \tag{10}$$

By applying the law of error propagation to equation 10, a covariance matrix of horizontal velocities in LG CS is computed as follows:

$$\mathbf{\Sigma}_{\mathbf{v}_i^p}^{(\mathrm{LG})} = \mathbf{K}_i^{(\mathrm{LG})} \mathbf{\Sigma}_{\mathbf{\Omega}^p} \mathbf{K}_i^{T(\mathrm{LG})} \tag{11}$$

where $\mathbf{\Sigma}_{\mathbf{\Omega}^p}$ in equation 11 is presumed as a diagonal matrix that is presented as:

$$\mathbf{\Sigma}_{\mathbf{\Omega}^p} = \mathrm{diag}\left(\sigma_{\Omega_{\mathrm{lat}}^p}^2, \sigma_{\Omega_{\mathrm{long}}^p}^2, \sigma_{\Omega^p}^2\right)$$

The covariance matrix of the velocities that is directly in LG CSS is given by equation (11), in which $\mathbf{K}_i^{(\mathrm{LG})}$ represents the Jacobian matrix of linearised observations that is the same as equation 10.

4.0 Application Development

Figure 3 shows the development phases of the PTC application. First and foremost, the phase starts with the initial design of the application interface, along with organising the sequence of input data formats using the open-source Visual Studio software. Based on the exploration of the formulations and parameters involved in Euler's theorem in the previous section, the results are translated into C# code compatible with Visual Studio and can be interpreted. Subsequently, the output data format has been organised into a comprehensive form, with both input and output data visualised in a ".txt" file. Following that, the About Us page and the user manual have been added as references and guidance for users during the implementation of the PTC. Lastly, after finalising the application interface design, the PTC is published in Visual Studio to convert it into a stand-alone application.

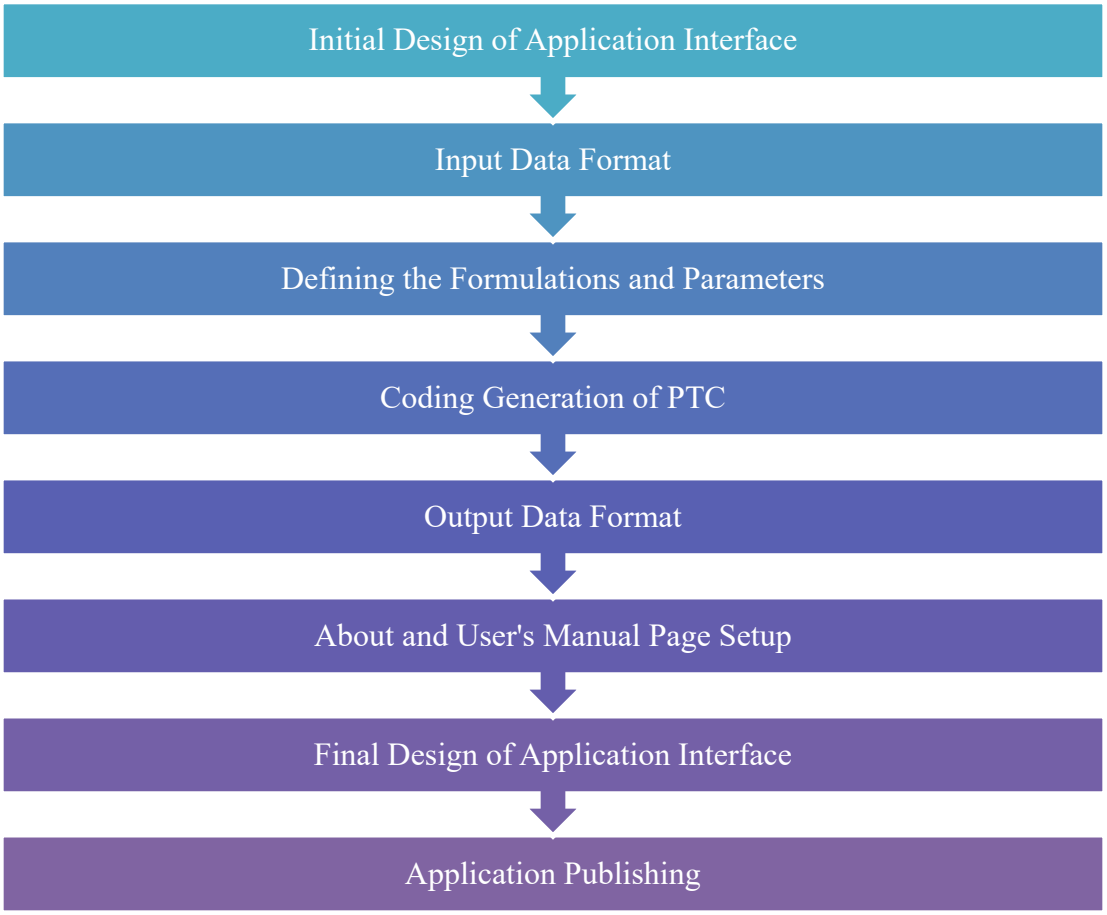

Figure 3. Process of Integrating the PTC

5.0 Plate Tectonic Calculator

Figure 4 illustrates the finalised user interface of the PTC, developed as a stand-alone application. The interface has been meticulously designed to be intuitive and user-centric, thereby eliminating unnecessary complexity and facilitating seamless navigation for users with varying levels of technical expertise. Complementing this, Figure 5 showcases the "About Us" section, which concisely introduces the PTC application's core objectives alongside relevant background information about its developer.

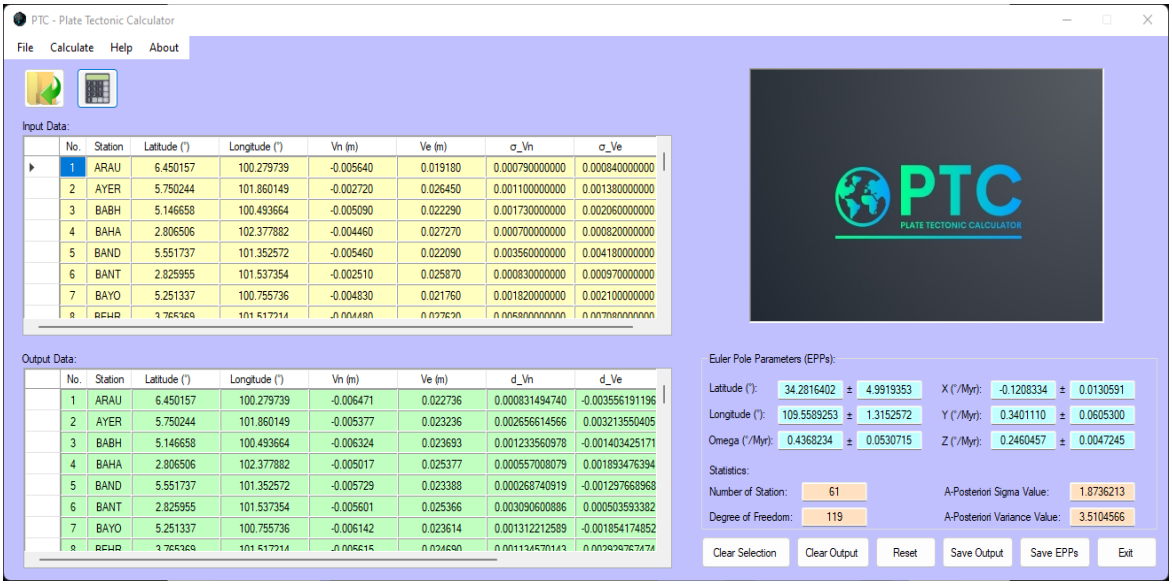

Figure 4. Interface of PTC

Figure 5. About Us Page of PTC

A critical prerequisite for ensuring optimal performance of the PTC is adherence to precise formatting of input data. The integrity and reliability of the application's output depend heavily on the correctness of the user-submitted data format. Any deviation from the specified format may lead to computational discrepancies or erroneous results. Consequently, users must strictly adhere to the input format requirements, as shown in Figure 6. Each parameter should be distinctly separated by spaces, tab characters, or commas to ensure accurate parsing. Furthermore, the input file must be provided with a ".txt" extension, commonly prepared in a plain-text editor such as Notepad, as demonstrated in Figure 7.

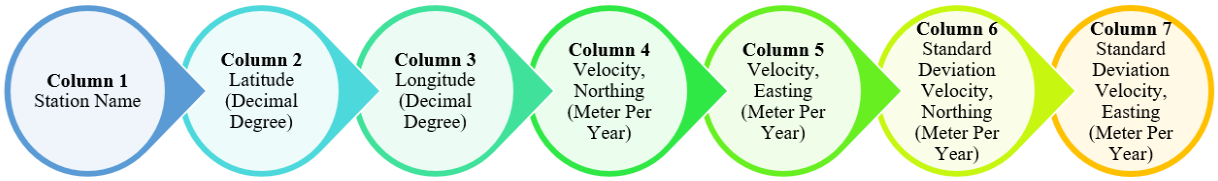

Figure 6. Input Data Format

Case 1 Input PTC.txt - Notepad

File Edit Format View Help

ALGO	45.955800	-78.071368	0.0020	-0.0162	0.000295127091	0.000286530976
AMC2	38.803124	-104.524594	-0.0050	-0.0139	0.001154945886	0.001276518703
ANNE	49.128231	-66.494615	0.0062	-0.0158	0.000496890330	0.000717147126
ATRI	46.847708	-71.261455	0.0049	-0.0168	0.000332114438	0.000445421149
BAIE	49.186827	-68.263328	0.0056	-0.0157	0.000216794834	0.000287228132
BAKE	64.317820	-96.002346	-0.0043	-0.0191	0.000386652299	0.000345398321
BARH	44.395048	-68.221691	0.0069	-0.0145	0.000197737199	0.000249198716
BCOM	49.187440	-68.261822	0.0062	-0.0164	0.000860348766	0.001261150269
BLYT	33.610415	-114.714851	-0.0090	-0.0140	0.000402492236	0.000263438797
BREW	48.131524	-119.682634	-0.0104	-0.0126	0.000185741756	0.000227596134
BRMU	32.370399	-64.696273	0.0076	-0.0121	0.000376430604	0.000417252921
CAGS	45.585021	-75.807328	0.0030	-0.0158	0.000279463772	0.000290344623
CAPL	48.093945	-65.652761	0.0068	-0.0154	0.000222036033	0.000401995025
CASA	37.644636	-118.896663	-0.0067	-0.0240	0.001480878118	0.000828673639

Figure 7. Example of Input Data Format in Notepad

Upon successful computation, users can export the generated results to designated file formats. The exportable output comprises two primary elements: the EPPs and the associated processed output data. As shown in Figures 8 and 10, both datasets can be saved in the standard

".txt" format, facilitating storage and further analysis. For clarity and consistency, the output parameter format follows the specific sequence shown in Figure 9.

EPPs_CASE 1.txt - Notepad

File Edit Format View Help

```
Euler Pole Parameters (EPPs):

Latitude(°):     -11.0429547      ±       1.2895904
Longitude (°):   -85.6623277      ±       0.5251187
Omega (°/Myr):   0.1760735        ±       0.0031520


Angular Velocities:

X (°/Myr):       0.0130706        ±       0.0016036
Y (°/Myr):       -0.1723183       ±       0.0039358
Z (°/Myr):       -0.0337260       ±       0.0046669
```

Figure 8. Example of Euler Pole Parameters Data Format in Notepad

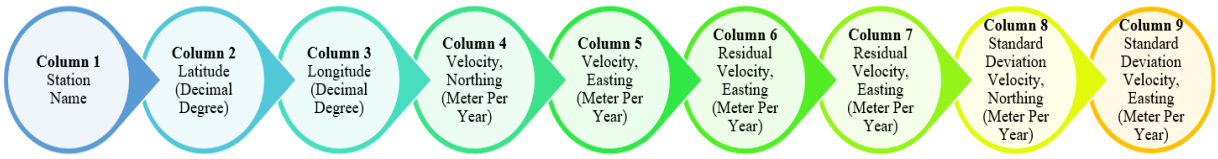

Figure 9. Output Data Format

Case 1 Output PTC.txt - Notepad

File Edit Format View Help

ALGO	45.955800	-78.071368	0.002538	-0.016299	-0.000538428590	0.000098616883	0.000184619375	0.000194417656
AMC2	38.803124	-104.524594	-0.006212	-0.014317	0.001212410976	0.000417471528	0.000217445196	0.000232790949
ANNE	49.128231	-66.494615	0.006309	-0.016179	-0.000109262161	0.000379077432	0.000221367315	0.000189968601
ATRI	46.847708	-71.261455	0.004779	-0.016143	0.000120900765	-0.000656814013	0.000203613836	0.000193797275
BAIE	49.186827	-68.263328	0.005746	-0.016329	-0.000146036756	0.000629154947	0.000214452372	0.000189359279
BAKE	64.317820	-96.002346	-0.003449	-0.018662	-0.000850938909	-0.000438347446	0.000189396875	0.000233946284
BARH	44.395048	-68.221691	0.005759	-0.015505	0.001140639398	0.001005104856	0.000214611117	0.000204028610
BCOM	49.187440	-68.261822	0.005747	-0.016329	0.000453481271	-0.000070861510	0.000214458110	0.000189358601
BLYT	33.610415	-114.714851	-0.009331	-0.012422	0.000331486697	-0.001578314397	0.000261208254	0.000279683053
BREW	48.131524	-119.682634	-0.010751	-0.014363	0.000351075685	0.001763401602	0.000283912514	0.000198258527
BRMU	32.370399	-64.696273	0.006876	-0.012774	0.000724244317	0.000674300113	0.000228718953	0.000282089537
CAGS	45.585021	-75.807328	0.003289	-0.016148	-0.000288914714	0.000347777000	0.000189914244	0.000196183589
CAPL	48.093945	-65.652761	0.006575	-0.015943	0.000224738570	0.000542788149	0.000224772125	0.000192621984
CASA	37.644636	-118.896663	-0.010532	-0.012786	0.003831588625	-0.011213837863	0.000280314492	0.000256838535

Figure 10. Example of Output Data Format in Notepad

The efficiency and accuracy of the PTC were rigorously validated through a comparative analysis with the established EPC, employing four distinct datasets sourced from prior research as test cases. The evaluation results, summarized in Table 1, highlight the comparative performance of output parameters across these datasets. Notably, the assessment reveals no significant discrepancies in the computed EPPs, angular velocities, station velocities, residuals, or the standard deviations in the northing and easting components. This consistency in output substantiates the operational reliability and computational integrity of the PTC, thereby endorsing its suitability for broader scientific applications.

Table 1. Analysis Table of Parameter Comparison

Cases	Calculation	Parameter	Result
All 4 Cases	Inverse Euler Pole Problem	EPPs Latitude (°)	No Significant Difference
		EPPs Longitude (°)	No Significant Difference
		EPPs Omega (°/Myr)	No Significant Difference
		Angular Velocities, X (°/Myr)	No Significant Difference
		Angular Velocities, Y (°/Myr)	No Significant Difference
		Angular Velocities, Z (°/Myr)	No Significant Difference
	Direct Euler Pole Problem	Velocity Northing, Vn	No Significant Difference
		Velocity Easting, Ve	No Significant Difference
		Residual Velocity Northing, dVn	No Significant Difference
		Residual Velocity Easting, dVe	No Significant Difference
		Standard Deviation Velocity Northing, σVn	No Significant Difference
		Standard Deviation Velocity Easting, σVe	No Significant Difference

Table 2 further delves into the EPPs derived from one of the four case datasets, providing a detailed comparison between the PTC and EPC outputs. The results demonstrate negligible variances in all EPPs and angular velocities. These marginal differences are attributable to the inherent characteristics of inverse matrix computations, which may vary slightly across platforms, since the PTC and EPC are developed in Visual Studio and MATLAB, respectively. Besides, the calculation process uses radian units and involves high-precision decimal values, which may lead to tiny deviations. However, after analysing the result, these small differences are acceptable and

within the uncertainties since they do not exceed the tolerance range of the standard deviation for all parameters. Therefore, it can be concluded that the formulations of EPPs and the performance of the PTC have been validated.

Figures 11, 12, and 13 illustrate the analysis graphs of output data for one of the four case datasets, presenting the comparative results in a visual form to provide a more comprehensive interpretation. Based on the graphs of the velocity differences between PTC and EPC, the discrepancies are less than 1×10^{-6} meters per year, indicating that the differences are acceptable. Additionally, the graphs of velocity residuals indicate that the discrepancies are below 1×10^{-9} meters per year. Apart from that, the graphs of velocity standard deviation also show the same trend as the velocity residuals, with all value discrepancies less than 1×10^{-9} meters per year. Therefore, it can be concluded that the value differences for all comparative parameters obtained from the PTC and EPC results are acceptable, as they are very small and lie within the uncertainties, thereby confirming the accuracy of the analysis and the validity of the PTC.

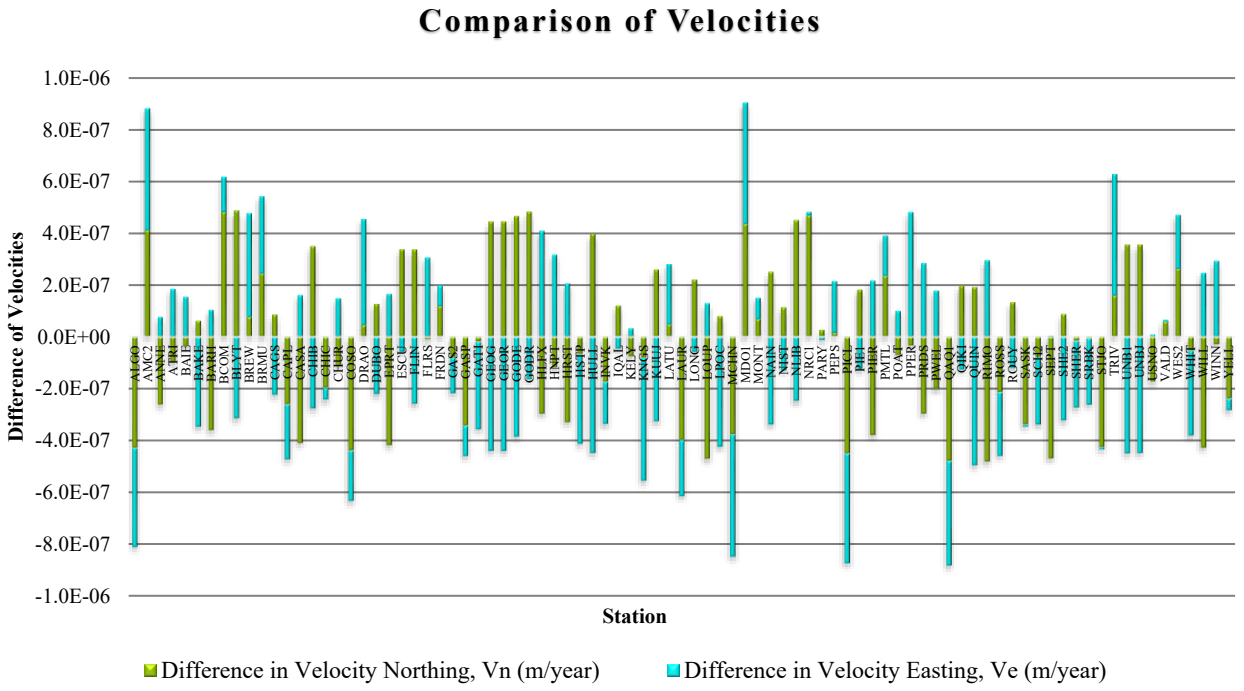

Figure 11. Analysis Graph of Velocities

Table 2. Analysis of EPPs

Euler Pole Parameters (EPPs):									
	PTC			**EPC**			**Difference**		
Latitude (°):	-11.0429547	±	1.2895904	-11.0429500	±	1.2895900	-0.000005	±	0.000000
Longitude (°):	-85.6623277	±	0.5251187	-85.6623300	±	0.5251200	0.000002	±	-0.000001
Omega (°/Myr):	0.1760735	±	0.0031520	0.1758800	±	0.0031500	0.000193	±	0.000002
Angular Velocities:									
	PTC			**EPC**			**Difference**		
X (°/Myr):	0.0130706	±	0.0016036	0.0129628	±	0.0016018	0.000108	±	0.000002
Y (°/Myr):	-0.1723183	±	0.0039358	-0.1719305	±	0.0039314	-0.000388	±	0.000004
Z (°/Myr):	-0.0337260	±	0.0046669	-0.0340594	±	0.0046618	0.000333	±	0.000005

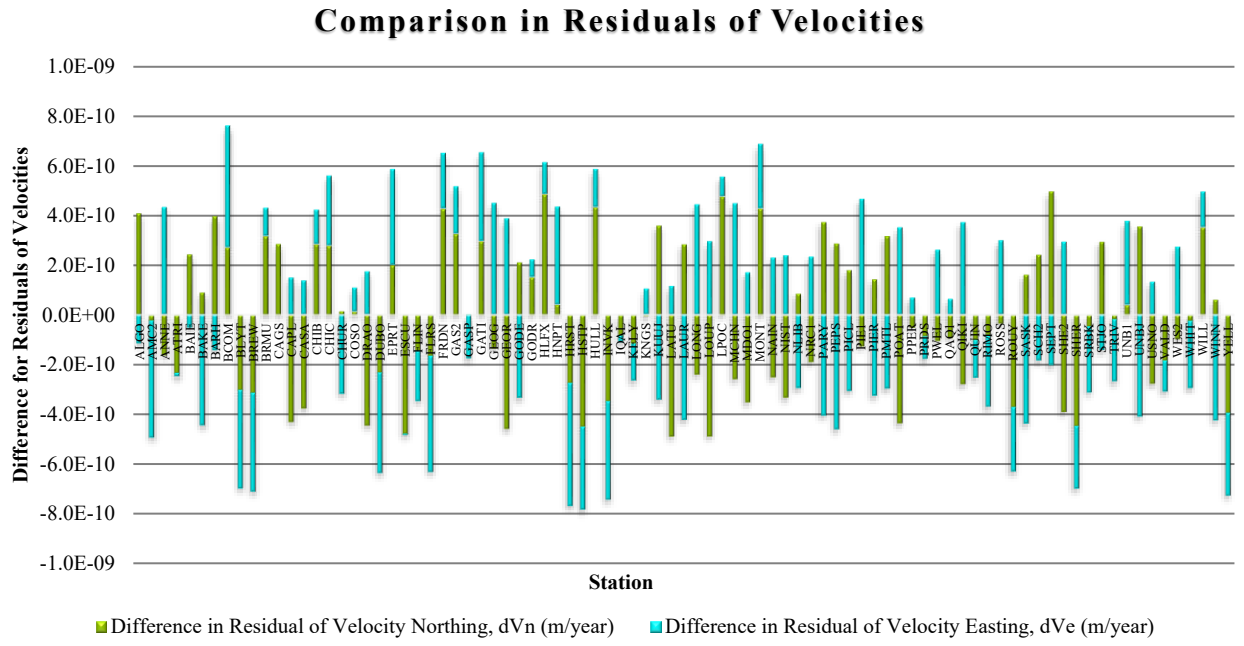

Figure 12. Analysis Graph of Velocities Residuals

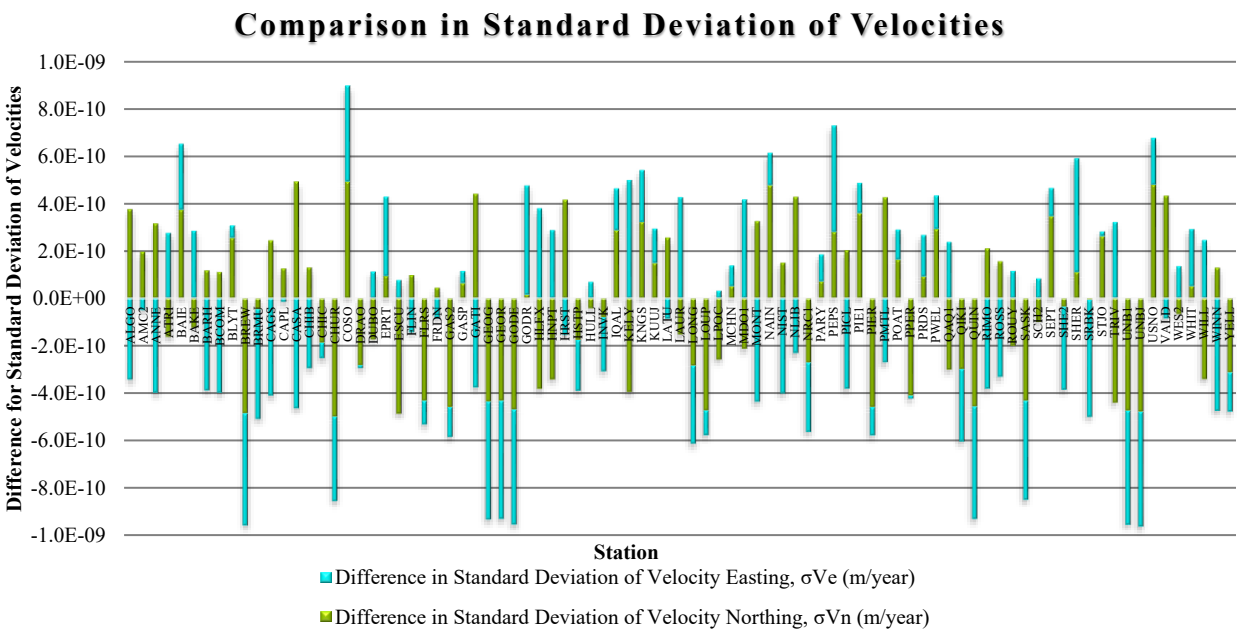

Figure 13. Analysis Graph of Velocities Standard Deviation

6.0 Conclusion

In conclusion, the PTC is meticulously developed to facilitate the computation of plate tectonic dynamics, with a primary focus on deriving EPPs. The foundational equations rooted in Euler's theorem were systematically reformulated into an integrated and structured approach. These equations bifurcate into two critical computational phases: the inverse and direct Euler pole problems in LG CS. These stages are instrumental for calculating EPPs and relative velocity, respectively. The mathematical formulations were initially validated through manual computations conducted using MATLAB to ensure precision and clarity in the algorithmic implementation. This verification phase was essential not only for confirming computational accuracy but also for gaining a comprehensive understanding of the algorithmic flow and source code architecture before integrating it into the PTC framework. The PTC was developed using Visual Studio and the C# programming language. Visual Studio was selected for its accessibility as an open-source integrated development environment that supports seamless deployment without licensing constraints.

Following successful manual validation, the software development process commenced, with deliberate attention to several critical components, which are designing a user-centric application interface, defining and validating input/output data format, integrating the computational formulas, generating efficient code, configuring navigation menus (including "About" and user guidance sections), and finalising the graphical user interface for public deployment. Each development phase is executed with precision to ensure seamless functionality and an optimal user experience. The existing EPC developed by Goudarzi et al. (2014) has been used for performance testing to compare results between PTC and EPC. As stated in the results and analysis section, there are no significant differences in the comparative parameters across the four case datasets. This is because the differences are acceptable and lie within the uncertainties. It does not exceed the standard deviation tolerance range for all evaluated parameters.

Therefore, it can be concluded that the PTC application's performance has been successfully verified. The results affirm that the developed tool stands as a reliable alternative for plate motion analysis, making it a valuable asset for geodynamic research. The PTC allows users to estimate plate tectonic motion that occurs in any region more efficiently by applying Euler pole computations. In addition, the PTC is developed as a stand-alone application that can be accessed

directly without requiring intermediary software. Moreover, the user can utilise the PTC without requiring a license key, and it is anticipated to be installed for free.

7.0 Future Outlook

Upon the conclusion of this study, several forward-looking recommendations have been identified to broaden the scope and elevate the functional capabilities of the PTC. These suggestions are intended to serve as a blueprint for future enhancements and to guide subsequent developments that build on the application's existing framework. Firstly, a pivotal enhancement would be the integration of statistical testing capabilities into the application. Incorporating statistical validation tools would facilitate a comprehensive assessment of model quality and robustness in EPP estimation. Statistical analyses such as the Chi-Square test, Pearson's correlation coefficient, Baarda's data snooping technique, and the Tau test can be embedded to rigorously evaluate the reliability and consistency of the output data.

Secondly, it is highly recommended that a data filtering module be embedded within the PTC to allow for the identification and exclusion of anomalous data points. The presence of outliers, particularly in station velocity datasets, can significantly distort the final results. By enabling users to detect and remove such deviations, the recalibration process can be conducted iteratively to ensure optimal accuracy in the resultant computations.

The third recommendation advocates incorporating a map canvas directly into the application's user interface. This enhancement would enable a graphical display of the global tectonic plate boundaries superimposed on a world map. By visualizing station locations alongside their respective velocity vectors, users would gain an intuitive spatial understanding of the plate motion data, thereby improving interpretability and user engagement.

Fourthly, the application could be expanded to support input data formatted in the ECEF CS. By allowing users to input data in ECEF CS rather than LG CS, the platform would provide greater flexibility and eliminate the need for prior coordinate transformations, streamlining the overall user experience. Lastly, a significant enhancement would be the development of a mobile version of the PTC. As mobile technology continues to advance rapidly, enabling the application to run on smartphones would greatly increase its accessibility and usability. Given the widespread reliance on mobile devices for both academic and professional tasks, transitioning the PTC to a mobile-compatible format would cater to the modern user's preference for portability and on-the-

go functionality, without compromising computational capabilities. In essence, these strategic recommendations aim to expand the versatility, analytical depth, and user accessibility of the PTC, thus positioning it as a comprehensive tool for future geodynamic analysis and plate tectonic motion research.

Acknowledgements

The authors would like to express their gratitude to Universiti Teknologi MARA, Perlis branch, for their encouragement towards this research. The reviews from anonymous readers in enhancing this article are deeply appreciated.

Conflicts of Interest

The author declares that there is no conflict of interest regarding the publication of this paper.

References

Adewale, Q., Khan, A. F., Carbonell, F., & Iturria-Medina, Y. (2021). Integrated transcriptomic and neuroimaging brain model decodes biological mechanisms in aging and Alzheimer's disease. *ELife*, *10*. https://doi.org/10.7554/eLife.62589

Andrews, D. L. (2003). Rice University Plate Motion Calculator. https://tectonics.rice.edu/calculators/hs3.html

Aneeshkumar, V., Indu, G. K., Santosh, M., James, S., Chandran, S. R., Padmakumar, D., & Sajinkumar, K. S. (2022). Terrestrial Impact Craters Track the Voyage of Lithospheric Plates. *Geological Journal*, *57*(9), 3769–3780. https://doi.org/10.1002/gj.4512

Blas, J. M. d., Iaffaldano, G., & Calais, E. (2022). Have the 1999 Izmit–Düzce Earthquakes Influenced the Motion and Seismicity of the Anatolian Microplate? *Geophysical Journal International*, *229*(3), 1754–1769. https://doi.org/10.1093/gji/ggac020

Cerpa, N. G., Sigloch, K., Garel, F., Heuret, A., Davies, D. R., & Mihalynuk, M. G. (2022). The Effect of a Weak Asthenospheric Layer on Surface Kinematics, Subduction Dynamics and Slab Morphology in the Lower Mantle. *Journal of Geophysical Research Solid Earth*, *127*(8). https://doi.org/10.1029/2022jb024494

Chen, L., Wang, X., Liang, X., Wan, B., & Liu, L. (2020). Subduction Tectonics vs. Plume Tectonics—Discussion on Driving Forces for Plate Motion. *Science China Earth Sciences*, *63*(3), 315–328. https://doi.org/10.1007/s11430-019-9538-2

Collot, J., Sutherland, R., Etienne, S., Patriat, M., Roest, W. R., Marcaillou, B., Clerc, C., Stratford, W., Mortimer, N., Juan, C., Bordenave, A., Schnürle, P., Barker, D. H. N., Williams, S., Wolf, S., & Crundwell, M. P. (2023). The Norfolk Ridge: A Proximal Record of the Tonga-Kermadec Subduction Initiation. *Geochemistry Geophysics Geosystems*, *24*(3). https://doi.org/10.1029/2022gc010721

Evora, A. J., Cocroft, R. B., Madhusudhana, S., & Hamel, J. A. (2024). VibePy: An open-source tool for conducting high-fidelity vibrational playback experiments. *Entomologia Experimentalis et Applicata*. https://doi.org/10.1111/eea.13500

Goudarzi, M. A., Cocard, M., & Santerre, R. (2014). EPC: Matlab Software to Estimate Euler Pole Parameters. *GPS Solutions*, *18*(1), 153–162. https://doi.org/10.1007/s10291-013-0354-4

Huang, S., Wang, W., Kerr, A. C., Zhao, J., Xiong, Q., & Wang, J. (2021). The Fuchuan Ophiolite in South China: Evidence for Modern-Style Plate Tectonics During Rodinia Breakup. *Geochemistry Geophysics Geosystems*, *22*(11). https://doi.org/10.1029/2021gc010137

Jagoda, M. (2021). Determination of Motion Parameters of Selected Major Tectonic Plates Based on GNSS Station Positions and Velocities in the ITRF2014. *Sensors*, *21*(16), 5342. https://doi.org/10.3390/s21165342

Koppers, A., Becker, T. W., Jackson, M. G., Konrad, K., Müller, R. D., Romanowicz, B., Steinberger, B., & Whittaker, J. M. (2021). Mantle Plumes and Their Role in Earth Processes. *Nature Reviews Earth & Environment*, *2*(6), 382–401. https://doi.org/10.1038/s43017-021-00168-6

Li, X., Wang, Q., Wu, J., Yuan, Y., Xiong, Y., Gong, X., & Wu, Z. (2022). Multi-GNSS products and services at iGMAS Wuhan Innovation Application Center: strategy and evaluation. *Satellite Navigation*, *3*(1). https://doi.org/10.1186/s43020-022-00081-3

Lowrie, W., & Fichtner, A. (2020). Fundamentals of Geophysics. In *Fundamentals of Geophysics*. Cambridge University Press. https://doi.org/10.1017/9781108685917

McCubbine, J. C., Riddell, A. R., & Brown, N. (2024). An Ellipsoidal Plate Motion Model of the Indo-Australian Tectonic Plate. *Journal of Geophysical Research: Solid Earth*, *129*(5), e2023JB027765. https://doi.org/https://doi.org/10.1029/2023JB027765

Müller, D., & Seton, M. (2016). Plate Motion. In *Encyclopedia of Earth Sciences Series: Vol. Part 2* (pp. 669–676). Springer Netherlands. https://doi.org/10.1007/978-94-007-6644-0_131-1

Mustafar, M. A., Simons, W. J. F., Tongkul, F., Satirapod, C., Omar, K. M., & Visser, P. N. A. M. (2017). Quantifying Deformation in North Borneo with GPS. *Journal of Geodesy*, *91*(10), 1241–1259. https://doi.org/10.1007/s00190-017-1024-z

NOAA. (2024). *What is Tectonic Shift?* National Ocean Service Website. https://oceanservice.noaa.gov/facts/tectonics.html

Parsons, A. J., Sigloch, K., & Hosseini, K. (2021). Australian Plate Subduction Is Responsible for Northward Motion of the India-Asia Collision Zone and ~1,000 km Lateral Migration of the Indian Slab. *Geophysical Research Letters*, *48*(18). https://doi.org/10.1029/2021gl094904

Tamaki, K., & Okino, K. (2018). Plate Motion Calculator. http://ofgs.aori.u-tokyo.ac.jp/~okino/platecalc_new.html

Wiel, E. v. d., Pokorný, J., Čížková, H., Spakman, W., Berg, A. P. van den, & Hinsbergen, D. J. v. (2024). Slab Buckling as a Driver for Rapid Oscillations in Indian Plate Motion and Subduction Rate. *Communications Earth & Environment*, *5*(1). https://doi.org/10.1038/s43247-024-01472-x

Zhang, K., Liao, J., & Gerya, T. (2024). Onset of Double Subduction Controls Plate Motion Reorganisation. *Nature Communications*, *15*(1). https://doi.org/10.1038/s41467-024-44764-8

Zhou, X., & Wada, I. (2022). Effects of Elasticity on Subduction Initiation: Insight From 2-D Thermomechanical Models. *Journal of Geophysical Research Solid Earth*, *127*(11). https://doi.org/10.1029/2022jb024400